

TOWARDS VISUAL DISTORTION IN BLACK-BOX ATTACKS

Nannan Li and Zhenzhong Chen*

School of Remote Sensing and Information Engineering, Wuhan University

ABSTRACT

Constructing adversarial examples in a black-box threat model injures the original images by introducing visual distortion. In this paper, we propose a novel black-box attack approach that can directly minimize the induced distortion by learning the noise distribution of the adversarial example, assuming only loss-oracle access to the black-box network. The quantified visual distortion, which measures the perceptual distance between the adversarial example and the original image, is introduced in our loss whilst the gradient of the corresponding non-differentiable loss function is approximated by sampling noise from the learned noise distribution. We validate the effectiveness of our attack on ImageNet. Our attack results in much lower distortion when compared to the state-of-the-art black-box attacks and achieves 100% success rate on ResNet50 and VGG16bn. The code is available at <https://github.com/Alina-1997/visual-distortion-in-attack>.

1 INTRODUCTION

Adversarial attack has been a well-recognized threat to existing deep neural network based applications. It injects small amount of noise to a sample (e.g., image, speech, language) but degrades the model performance drastically [1, 2, 3]. According to the information that an adversary has of the target network, existing attack falls into two categories: white-box attack that knows all the parameters of the target network, and black-box attack that only has access to the output of the target network. However, it's sometimes difficult or even impossible to have full access to certain networks, which makes the black-box attack practical and attract more and more attention.

Black-box attack has very limited or no information of the target network and thus is more challenging to perform. In the l_p -bounded setting, a black-box attack is usually evaluated on two aspects: number of queries and success rate. In addition, recent work [4] shows that visual distortion in the adversarial examples is also an important criteria in practice. Even under a small l_∞ bound, perturbing pixels in the image without considering the visual impact could make the distorted image very annoying. As shown in Fig. 1, an attack [5] under a small noise level ($l_\infty \leq 0.05$) causes relatively large visual distortion and the perturbed image is more distinguishable from the original one. Therefore, under the assumption that the visual distortion caused by the noise is related to the spatial distribution of the perturbed pixels in a bounded l_p attack, we take a different view from previous work and focus on *explicitly* learning a noise distribution based on its corresponding visual distortion.

In this paper, we propose a novel black-box attack that can directly minimize the induced visual distortion by learning the noise distribution of the adversarial example, assuming only loss-oracle access to the black-box network. The quantified visual distortion, which measures the perceptual distance between the adversarial example and the original image, is introduced in our loss where the gradient of the corresponding non-differentiable loss function is approximated by sampling noise from the learned noise distribution. The proposed attack can achieve a trade-off between visual distortion and query efficiency by introducing the weighted perceptual distance metric in addition to the original loss. Theoretically, we prove the convergence of our model under the assumption that the loss function

is convex. The experiments demonstrate the effectiveness of our attack on ImageNet. Our attack results in much lower distortion than the other attacks and achieves 100% success rate on ResNet50 and VGG16bn. In addition, it is shown that our attack is valid even when it's only allowed to perturb pixels that are out of the target object in a given image.

2 RELATED WORK

Although adversarial attack poses a big threat to existing networks, performing attacks can evaluate the robustness of a network, and further helps improve its robustness by augmenting adversarial examples in training [6]. Recent research on the adversarial attack has made advanced progress in developing a stronger and more computationally efficient adversary. Since our method is based on black-box attack, we briefly introduce recent attack techniques in the black-box setting.

Black-box attack considers the target network as a black-box, and only assumes access to its output scores. Existing methods for the black-box attack roughly fall into three categories: 1) Methods that estimate gradient of the black-box. Some methods estimate the gradient by sampling around a certain point, which formulates the task as a problem of continuous optimization. Tu *et al.* [7] searched for perturbations in the latent space of an auto-encoder. Ilyas *et al.* [5] exploited prior information about the gradient. Al-Dujaili and O'Reilly [8] reduced query complexity by estimating just the sign of the gradient. [9] shares similarity with our method as it also *explicitly* defines a noise distribution. However, the distribution in [9] is assumed to be an isometric normal distribution without considering visual distortion whilst our method does not assume the distribution to be a specific form and learns a noise distribution that causes less visual distortion. Other approaches developed a substitute model [3, 10, 11] to approximate performance of the black-box. By exploiting the transferability of adversarial attack [12], the white-box attack technique applied to the substitute model can be transferred to the black-box. These approaches assume only label-oracle to the black-box, whereas training of the substitute model requires either access to the black-box training dataset or collection of a new dataset. 2) Methods based on discrete optimization. In [13, 8], an image is divided into regular grids and the attack is performed and refined on each grid. Meunier *et al.* [14] adopted

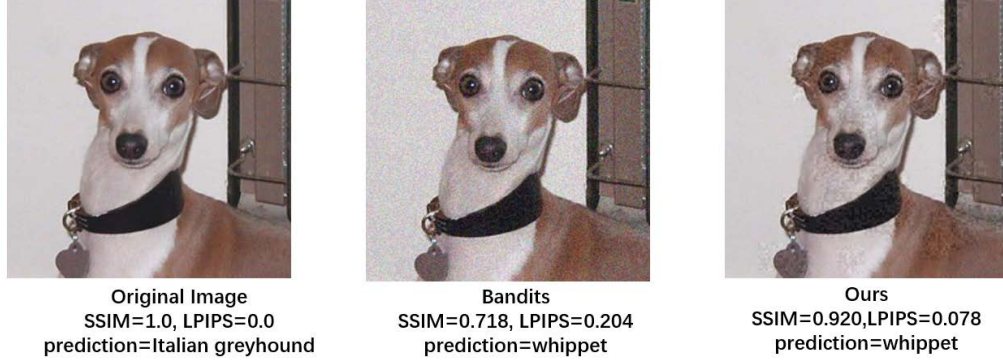


Figure 1: Adversarial examples on ImageNet with bounded noise $\|\delta\|_\infty \leq 0.05$. The first image is the original unperturbed image. The following examples are from [5] and our method, respectively. Higher SSIM and lower LPIPS indicate less visual distortion.

Algorithm 1: Our Algorithm

Input: image x , maximum norm ϵ , proportion q of the resampled noise

Output: adversarial example $x + \delta$

```

1 Initialize noise distribution  $p_{\theta_0} = \text{softmax}(\theta_0)$  and noise  $\delta_0$ 
2 for step  $t$  in  $\{1, \dots, n\}$  do
3    $T^* = \text{argmin}_{T=0,1,\dots,t-1} L(x, x + \delta_T)$ 
4   Compute baseline  $b = L(x, x + \delta_{T^*})$ 
5   Update  $\theta$  using Eq. (17),  $\theta_t \leftarrow \theta_{t-1} - \nabla F(\theta_{t-1})$ 
6   Sample  $\delta_t$ ,
       $\delta_t \leftarrow \text{sample}(\delta_t, q)_{\delta_t \sim p_{\theta_t}} \cup \text{sample}(\delta_{T^*}, 1 - q)_{\delta_{T^*} \sim p_{\theta_{T^*}}}$ 
7   if successful_attack( $x, x + \delta_t$ ) then
8     return  $x + \delta_t$ 
9 def successful_attack( $x, x + \delta_t$ ):
10  if  $\text{argmax}_{k_1} f(x + \delta_t)_{k_1} \neq \text{argmax}_{k_2} f(x)_{k_2}$  then
11    return True
12  else
13    return False

```

the tiling trick by adding the same noise for small square tiles in the image. 3) Methods that leverage evolutionary strategies or random search [14, 15]. In [15], the noise value is updated using a square-shaped random search at each query. Meunier *et al.* [14] developed a set of attacks using evolutionary algorithms using both continuous and discrete optimization.

Previous methods did not consider the visual impact of the induced noise, for which the adversarial example could suffer from significant visual distortion. This motivates us to consider the visual quality degradation in the attack model. Under the assumption that the visual distortion caused by the noise is related to the spatial distribution of the perturbed pixels in a bounded l_p attack, we *explicitly* define a noise distribution, which is learned to minimize the visual distortion.

3 METHOD

3.1 Learning Noise Distribution Based on Visual Distortion

An attack model is an adversary that constructs adversarial examples against certain networks. Let $f : x \rightarrow f(x)$ be the target

network that accepts an input $x \in \mathbb{R}^n$ and produces an output $f(x) \in \mathbb{R}^m$. $f(x)$ is a vector and $f(x)_k$ represents its k th entry, denoting the score of the k th class. $y = \text{argmax}_k f(x)_k$ is the predicted class. Given a valid input x and the corresponding predicted class y , an adversarial example [16] x' is similar to x yet results in an incorrect prediction $\text{argmax}_k f(x')_k \neq y$. In an additive attack, an adversarial example x' is a perturbed input with additive noise δ such that $x' = x + \delta$, where δ is bounded by an l_p ball. Although there are several choices of p ($p = 0, 1, 2, \infty$), we discuss l_∞ in this paper since our method defines a sample space with a fixed range for each pixel independently. As for other p values, please refer to section 4.5 for further discussions. The problem of generating an adversarial example is equivalent to produce noise δ that causes wrong prediction for the perturbed input. Thus a successful attack is to find δ such that (1) $\text{argmax}_k f(x + \delta)_k \neq y$ and (2) $\|\delta\|_\infty \leq \epsilon$. Since the constraint (1) is highly non-linear, the problem is usually rephrased in a different form [1]:

$$\begin{aligned} & \underset{\delta}{\text{minimize}} \quad L(x, x + \delta) \\ & \text{subject to} \quad \|\delta\|_\infty \leq \epsilon \end{aligned} \quad (1)$$

where $L(x, x + \delta)$ is the loss function, which is defined as $\max(0, f(x + \delta)_y - \max_{k \neq y} f(x + \delta)_k)$. The attack is successful when $L = 0$. It's noted that such a loss does not take the visual impact into consideration, for which the adversarial example could suffer from significant visual distortion. In order to constrain the visual distortion caused by the difference between x and $x + \delta$, we adopt a perceptual distance metric $d(x, x + \delta)$ into the loss function with a predefined hyperparameter λ :

$$\begin{aligned} L(x, x + \delta) = & \max(0, f(x + \delta)_y - \max_{k \neq y} f(x + \delta)_k) \\ & + \lambda d(x, x + \delta) \end{aligned} \quad (2)$$

where smaller $d(x, x + \delta)$ indicates less visual distortion. d can be any form of metric that measures the perceptual distance between x and $x + \delta$, such as well established $1 - \text{SSIM}$ [17] or LPIPS [18]. λ manages the trade-off between a successful attack and the visual distortion caused by the attack. The effects of λ will be further discussed in Section 4.1.

Minimizing the above loss function facing a challenge that L is not differentiable since the black-box adversary does not have access to the gradients of L and the predefined $d(x, x + \delta)$ might be calculated in a non-differentiable way. To address this problem, we *explicitly* assume a noise distribution of δ and approximate

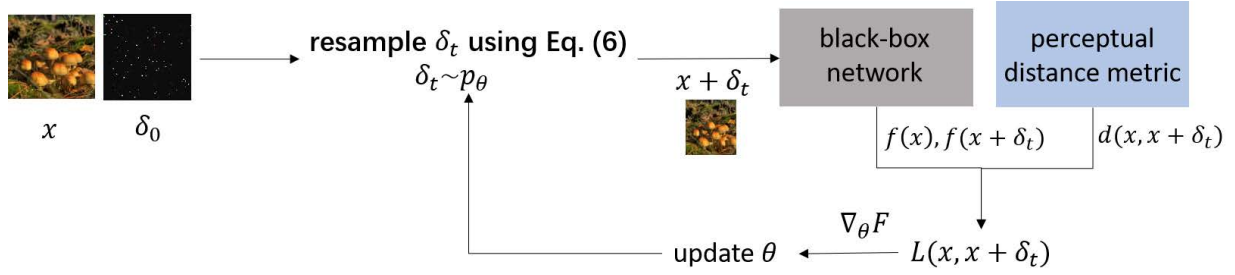


Figure 2: Framework of the proposed attack.

the gradient of L by sampling from the distribution. Suppose that δ follows a distribution p_θ parameterized by θ , i.e., $\delta \sim p_\theta$. For the j th pixel in an image, we make its noise distribution $p_{\theta^j} = \text{softmax}(\theta^j)$, where θ^j is the j th component of θ . The noise value δ_j of the j th pixel is sampled by following p_{θ^j} . By sampling noise from the distribution, θ can be learned to minimize the expectation of the above loss such that the attack is successful (i.e., alters the predicted label) and the produced adversarial example is less distorted (i.e., small d). The expectation is minimized by sampling δ from p_θ for each pixel:

$$\begin{aligned} & \text{minimize } \mathbb{E}_{\delta \sim p_\theta} [L(x, x + \delta)] \\ & \text{subject to } \|\delta\|_\infty \leq \epsilon \end{aligned} \quad (3)$$

To ensure the l_∞ constraint is satisfied, we define the sample space of noise δ^j for the j th pixel to be a set of discrete values in the range of $-\epsilon$ and ϵ : $\delta^j \in \{\epsilon, \epsilon - \frac{\epsilon}{N}, \epsilon - 2\frac{\epsilon}{N}, \dots, 0, \dots, -\epsilon\}$, where N is the sampling frequency and $\frac{\epsilon}{N}$ is the sampling interval. The noise value δ_j of the j th pixel is sampled from this sample space by following p_{θ^j} .

Given w and h the width and height of an image, respectively, since each pixel has its own noise distribution p_{θ^j} of length $2N + 1$, the length of p_θ for the entire image is $(2N + 1)wh$. Note that we do not consider the difference of color channels. Thus, the same noise value is sampled for each color channel of a pixel. To estimate θ , we adopt policy gradient [19] to make the above expectation differentiable with respect to θ . Using REINFORCE, we have the differentiable loss function $F(\theta)$:

$$\begin{aligned} F(\theta) &= \mathbb{E}_{\delta \sim p_\theta} [L(x, x + \delta) - b] \\ &= (L(x, x + \delta) - b) \log(p_\theta(\delta)) \end{aligned} \quad (4)$$

$$\begin{aligned} \nabla F(\theta) &= \nabla_\theta \mathbb{E}_{\delta \sim p_\theta} [L(x, x + \delta) - b] \\ &= (L(x, x + \delta) - b)(1 - p_\theta(\delta)) \end{aligned} \quad (5)$$

where b is introduced as a *baseline* in the expectation with specific meaning: 1) when $L(x, x + \delta) < b$, the sampled δ returns low L , and its probability $p_\theta(\delta)$ increases through gradient descent; 2) when $L(x, x + \delta) = b$, $\nabla F(\theta) = 0$ and $p_\theta(\delta)$ remains unchanged; 3) when $L(x, x + \delta) > b$, the sampled δ returns high L , and its probability $p_\theta(\delta)$ decreases through gradient descent. To sum up, $L(x, x + \delta)$ is forced to improve over b . At the iteration t , we choose $b = \min_{T=0,1,\dots,t-1} L(x, x + \delta_T)$ such that L improves over the obtained minimal loss.

The above expectation is estimated using a single Monte Carlo sampling at each iteration, and the sampling of noise δ is critical. Simply sampling δ_t at the iteration t on the entire image might cause large variance on the norm of the noise, i.e., $\|\delta_t - \delta_{t-1}\|_2$. Therefore, to ensure a small variance, with

$T^* = \text{argmin}_{T=0,1,\dots,t-1} L(x, x + \delta_T)$, only a small proportion of the noise is randomly resampled from iteration T^* while the others remain unchanged. Let q be the proportion of the resampled noise at each iteration, the updated δ_t at an iteration t is

$$\delta_t \leftarrow \text{sample}(\delta_t, q)_{\delta_t \sim p_{\theta_t}} \cup \text{sample}(\delta_{T^*}, 1 - q)_{\delta_{T^*} \sim p_{\theta_{T^*}}} \quad (6)$$

where $\text{sample}(\delta_t, q)$ denotes randomly sampling proportion q of the noise from δ_t . As shown in Fig. 2, at the iteration t , proportion q of noise δ_t is resampled by following the corresponding distribution p_{θ_t} . Then, the feedback $L(x, x + \delta_t)$ from the black-box and the perceptual distance metric decide the update of the distribution p_{θ_t} . The iteration stops when the attack is successful, i.e., $\max(0, f(x + \delta_t)_y - \max_{k \neq y} f(x + \delta_t)_k) = 0$.

3.2 Proof of Convergence

Ruan *et al.* [20] shows that feed-forward DNNs (Deep Neural Networks) are Lipschitz continuous with a Lipschitz constant K . Therefore, we have

$$\forall t_1, t_2, \|f(x + \delta_{t_1}) - f(x + \delta_{t_2})\|_2 \leq K \|\delta_{t_1} - \delta_{t_2}\|_2 \quad (7)$$

Let $t_1 = t$ and $t_2 = T^*$, where $T^* = \text{argmin}_{T=0,1,\dots,t-1} L(x, x + \delta_T)$, we have

$$\forall t, \|f(x + \delta_t) - f(x + \delta_{T^*})\|_2 \leq K \|\delta_t - \delta_{T^*}\|_2 \quad (8)$$

At an iteration t , since only a small proportion of the noise is randomly resampled from iteration T^* , it can be assumed that

$$|\max_{k \neq y} f(x + \delta_t)_k - \max_{k \neq y} f(x + \delta_{T^*})_k| \leq C \quad (9)$$

where C is a constant. Note that the learning stops when the attack is successful, i.e., $\max(0, f(x + \delta_t)_y - \max_{k \neq y} f(x + \delta_t)_k) = 0$. Therefore, $\max(0, f(x + \delta_t)_y - \max_{k \neq y} f(x + \delta_t)_k) = f(x + \delta_t)_y - \max_{k \neq y} f(x + \delta_t)_k > 0$ until the learning stops. Suppose that the perceptual distance metric d is normalized to $[0, 1]$. Substituting the inequalities (8) and (9) in our definition of L in Eq. (2) gets the following inequality:

$$\begin{aligned} & |L(x, x + \delta_t) - L(x, x + \delta_{T^*})| \\ & \leq |\max_{k \neq y} f(x + \delta_t)_k - \max_{k \neq y} f(x + \delta_{T^*})_k| \\ & \quad + |f(x + \delta_t)_y - f(x + \delta_{T^*})_y| \\ & \quad + \lambda |d(x, x + \delta_t) - d(x, x + \delta_{T^*})| \\ & \leq K \|\delta_t - \delta_{T^*}\|_2 + C + \lambda \end{aligned} \quad (10)$$

Note that $\|\delta_t\|_\infty$ is bounded by ϵ . Given width w , height h , channel c of the image, and the resampled proportion q of the noise from iteration T^* , we have

$$\|\delta_t - \delta_{T^*}\|_2 \leq 2\epsilon whcq \quad (11)$$

Thus, the inequality (10) becomes

$$|L(x, x + \delta_t) - L(x, x + \delta_{T^*})| \leq 2K\epsilon whcq + C + \lambda \quad (12)$$

Ideally, $L(x, x + \delta_t) - L(x, x + \delta_{T^*})$ accurately quantifies the difference of the perturbed image even when only one noise value for just a single pixel at the iteration t is sampled differently from that at T^* . Let $x + \delta_t^{ij}$ represent the perturbed image with the i th noise value of the j th pixel being sampled. Note that θ is a vector of length $(2N + 1) \cdot wh$, denoting that there are $(2N + 1)$ noise values that could be sampled for each pixel. Similarly, $p_\theta(\delta_t^{ij})$ denotes the probability of the i th noise value of the j th pixel being sampled. By sampling every noise value for the j th pixel, we define l_t^j and $p_{\theta_t^j}$ to be a vector:

$$\forall j \in \{1, 2, \dots, wh\}, l_t^j = \text{vector}[L(x, x + \delta_t^{ij}) - L(x, x + \delta_{T^*})], \\ i = 1, 2, \dots, 2N + 1 \quad (13)$$

$$\forall j \in \{1, 2, \dots, wh\}, p_{\theta_t^j} = \text{vector}[p_\theta(\delta_t^{ij})], \\ i = 1, 2, \dots, 2N + 1 \quad (14)$$

Although the above equations are only meaningful under the ideal situation where L can quantify the difference of just one perturbed pixel, we use these equations for a theoretical proof of convergence. In the ideal situation, instead of using a single Monte Carlo sampling to estimate $\nabla F(\theta_t)$ as in Eq. (5), the j th component of $\nabla F(\theta_t)$ can be calculated exactly as

$$\nabla F(\theta_t^j) = l_t^j \cdot (1 - p_{\theta_t^j}) \quad (15)$$

where $\nabla F(\theta_t^j)$ is the j th component of $\nabla F(\theta_t)$. According to Eq. (12) when the number of the resampled pixels $whq=1$, we have

$$|L(x, x + \delta_t^{ij}) - L(x, x + \delta_{T^*})| \leq 2K\epsilon c + C + \lambda \quad (16)$$

Note that for $\forall t_1, t_2$ that share the same T^* , $l_{t_1}^j$ is equal to $l_{t_2}^j$. Thus, replacing the inequality (18) in Eq. (17) gets

$$\begin{aligned} & \|\nabla F(\theta_{t_1}^j) - \nabla F(\theta_{t_2}^j)\|_2 \\ & \leq \|l_{t_1}^j\|_2 \|(\mathbf{1} - p_{\theta_{t_1}^j}) - (\mathbf{1} - p_{\theta_{t_2}^j})\|_2 \\ & \leq (2N + 1)(2K\epsilon c + C + \lambda) \|p_{\theta_{t_1}^j} - p_{\theta_{t_2}^j}\|_2 \\ & = (2N + 1)(2K\epsilon c + C + \lambda) \|\text{softmax}(\theta_{t_1}^j) - \text{softmax}(\theta_{t_2}^j)\|_2 \end{aligned} \quad (17)$$

In practice, we adopt a single Monte Carlo sampling instead of sampling every noise values for every pixel, for which $2N + 1$ should be replaced by 1 in the above inequality. The inequality (17) thus becomes:

$$\begin{aligned} & \|\nabla F(\theta_{t_1}^j) - \nabla F(\theta_{t_2}^j)\|_2 \\ & \leq (2K\epsilon c + C + \lambda) \|\text{softmax}(\theta_{t_1}^j) - \text{softmax}(\theta_{t_2}^j)\|_2 \end{aligned} \quad (18)$$

Since the standard softmax function is Lipschitz continuous with the Lipschitz constant being 1 [21]. We have

$$\|\nabla F(\theta_{t_1}^j) - \nabla F(\theta_{t_2}^j)\|_2 \leq (2K\epsilon c + C + \lambda) \|\theta_{t_1}^j - \theta_{t_2}^j\|_2 \quad (19)$$

Finally, the inequality for $\|\nabla F(\theta_{t_1}) - \nabla F(\theta_{t_2})\|_2$ becomes

$$\begin{aligned} & \|\nabla F(\theta_{t_1}) - \nabla F(\theta_{t_2})\|_2 \\ & = \sqrt{\sum_{j=1}^{wh} \|\nabla F(\theta_{t_1}^j) - \nabla F(\theta_{t_2}^j)\|_2^2} \\ & \leq (2K\epsilon c + C + \lambda) \sqrt{\sum_{j=1}^{wh} \|\theta_{t_1}^j - \theta_{t_2}^j\|_2^2} \\ & = (2K\epsilon c + C + \lambda) \|\theta_{t_1} - \theta_{t_2}\|_2 \end{aligned} \quad (20)$$

The above inequality proves that $F(\theta)$ is L -smooth with the Lipschitz constant being $2K\epsilon c + C + \lambda$. Assuming that $F(\theta)$ is convex, according to the convergence theorem for gradient descent [22], it follows that

$$F(\theta_t) - F(\theta^*) \leq \frac{(2K\epsilon c + C + \lambda) \cdot \|\theta_0 - \theta^*\|_2^2}{t} \quad (21)$$

where θ^* is the optimal solution. When t is large enough, $F(\theta_t)$ approximates $F(\theta^*)$ up to a small enough epsilon and the learning converges.

4 EXPERIMENTS

Following previous work [14, 5], we validate the effectiveness of our model on the large-scale ImageNet [23] dataset. We use three pretrained classification networks on Pytorch as the black-box networks: InceptionV3 [24], ResNet50 [25] and VGG16bn [26]. The attack is performed on images that were correctly classified by the pretrained network. We randomly select 1000 images in the validation set for test, and all images are normalized to $[0, 1]$. We quantify our success in terms of the perceptual distance (1 - SSIM and LPIPS) as we address the visual distortion caused by the attack. In these two metrics, 1 - SSIM [17] measures the degradation of structural information in the adversarial examples. Smaller 1 - SSIM indicates closer perceptual distance. LPIPS [18] evaluates the perceptual similarity of two images with their normalized distance between their deep features. Smaller value of LPIPS denotes less visual distortion. Except for 1 - SSIM and LPIPS, the success rate and average number of queries are also reported as in most frameworks. The average number of queries refers to the average number of requests to the output of the black-box network.

We initialize the noise distribution p_θ to be a uniform distribution and noise δ_0 to be 0. The learning rate is 0.01 and q is set to be 0.01. In addition, we specify the shape of the resampled noise at each iteration to be a square [14, 13, 15], and adopt the tiling trick [5, 14] with tile size= 2. The upper bound ϵ of our attack is set to be 0.05 as in previous work.

4.1 Ablation Studies

In the ablation studies, the maximum number of queries is set to be 10,000. The results are averaged on 1000 test images. In the following, we discuss the trade-off between visual distortion and query efficiency, the effects of using different perceptual distance metrics in the loss function and the results on different sampling frequencies.

Table 1: Ablation results of the perceptual distance metric, λ and sampling frequency N . Smaller $1 - \text{SSIM}$ and LPIPS indicate less visual distortion.

Sampling Frequency	Perceptual Metric	λ	Success Rate	$1 - \text{SSIM}$	LPIPS	Avg. Queries
$N = 1$	-	0	100%	0.091	0.099	356
	$1 - \text{SSIM}$	10	100%	0.076	0.081	401
		100	97.4%	0.036	0.051	1395
		200	92.2%	0.025	0.040	2534
	LPIPS	10	100%	0.080	0.078	450
		100	98.1%	0.049	0.052	1174
		200	95.1%	0.038	0.045	1928
$N = 2$	$1 - \text{SSIM}$	10	99.7%	0.071	0.074	520
$N = 5$	$1 - \text{SSIM}$	10	99.5%	0.069	0.070	665
$N = 10$	$1 - \text{SSIM}$	10	98.7%	0.062	0.075	669
$N = 12$	$1 - \text{SSIM}$	10	98.7%	0.071	0.075	673

Trade-off between visual distortion and query efficiency.

Under the same l_∞ ball, a query-efficient way to produce an adversarial example is to perturb most pixels with the maximum noise values $\pm\epsilon$ [13, 15]. However, such attack introduces large visual distortion, which could make the distorted image very annoying. To constrain the visual distortion, the perturbed pixels should be those who cause smaller visual difference while performing a valid attack, which takes extra queries to find. This brings the trade-off between visual distortion and query efficiency. Different from previous work, this trade-off can be controlled by λ in our loss function. As shown in Table 1, when $N = 1$ and $\lambda = 0$, the adversary does not consider visual distortion at all, and perturbs each pixel that is helpful for misclassification until the attack is successful. Thus, it causes the largest perceptual distance (0.081 and 0.089) with the least number of queries (356). As λ increases to 200, both $1 - \text{SSIM}$ and LPIPS decrease at the cost of more queries and lower success rate. The maximum λ in Table 1 is 200 since further increasing it causes the success rate to be lower than 90%. Fig. 3 gives several visualized examples on different λ , where adversarial examples with larger λ suffer from less visual distortion.

Ablation studies on the perceptual distance metric. The perceptual distance metric d in the loss function is predefined to measure the visual distortion between the adversarial example and the original image. We adopt $1 - \text{SSIM}$ and LPIPS as the perceptual distance metric to optimize, respectively, and report their results in Table 1. When $\lambda = 10$, optimizing $1 - \text{SSIM}$ shows better score on $1 - \text{SSIM}$ (0.066 v.s. 0.070) whilst optimizing LPIPS has better performance on LPIPS (0.068 v.s. 0.071). However, when λ increases to 100 and 200, optimizing $1 - \text{SSIM}$ gives better scores on both $1 - \text{SSIM}$ and LPIPS. Therefore, we set the perceptual distance metric to be $1 - \text{SSIM}$ in the following experiments.

Sampling frequency. Sampling frequency decides the size of the sample space of δ . Setting higher frequency means there are more noise values to explore through sampling. In Table 1, increasing the sampling frequency from $N = 1$ to $N = 2$ reduces the perceptual distance to some extent at the cost of

lower success rate. On the other hand, further increasing N to 12 does not essentially reduce the distortion yet lowers the success rate. To ensure a high success rate of attack, we set the sampling frequency $N = 1$ in the following experiments. Note that the maximum sampling frequency is $N = 12$ because the sampling interval in RGB color space (*i.e.*, $255 * 0.05/N$) would be less than 1 if $N > 12$. See Fig. 4 for a few adversarial examples.

4.2 Out-of-Object Attack

Most existing classification networks [25, 27] are based on CNN (Convolutional Neural Network), which gradually aggregates contextual information in deeper layers. Therefore, it is possible to fool the classifier by just attacking the “context”, *i.e.*, background that is out of the target object. Attacking just the out-of-object pixels constrains the number and the position of pixels that can be perturbed, which might further reduce the visual distortion caused by the noise. To locate the object in a given image, we exploited the object bounding box provided by ImageNet. An out-of-object mask is then created according to the bounding box such that the model is only allowed to attack pixels that are out of the object, as shown in Fig. 5. In Table 2, we report results of InceptionV3, ResNet50 and VGG16bn with the maximum queries= 40,000. The attack is performed on images whose masks are at least 10% large of the image area. The results show that attacking just the out-of-object pixels can also cause misclassification of the object with over 90% success rate. Compared with image attack, the out-of-object attack is more difficult for the adversary in that it requires more number of queries (4275/3775/3104) yet has lower success rate (90.1%/93.8%/94.7%). On the other hand, the out-of-object attack indeed reduces visual distortion of the adversarial examples on the three networks.

4.3 Attack Effectiveness on Defended Network

In the above experiments, we show that our black-box model can attack the *undefended* network with high success rate. To evaluate the strength of the proposed attack in *defended* situation, we further attack the InceptionV3 network that adopts

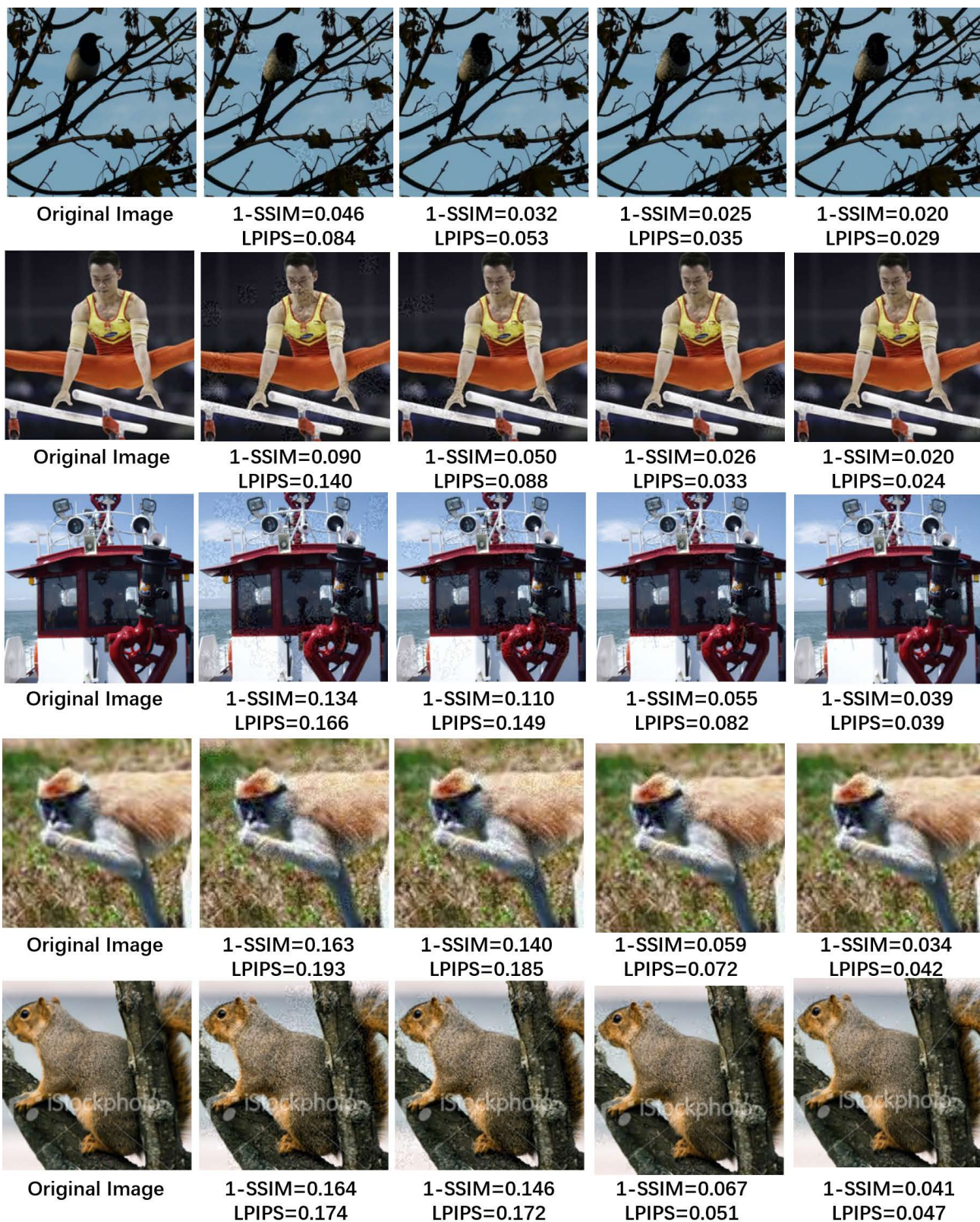


Figure 3: Visualized examples of the proposed attack. From left to right is the original image, the adversarial examples on $\lambda = 0, \lambda = 10, \lambda = 100, \lambda = 200$, respectively.

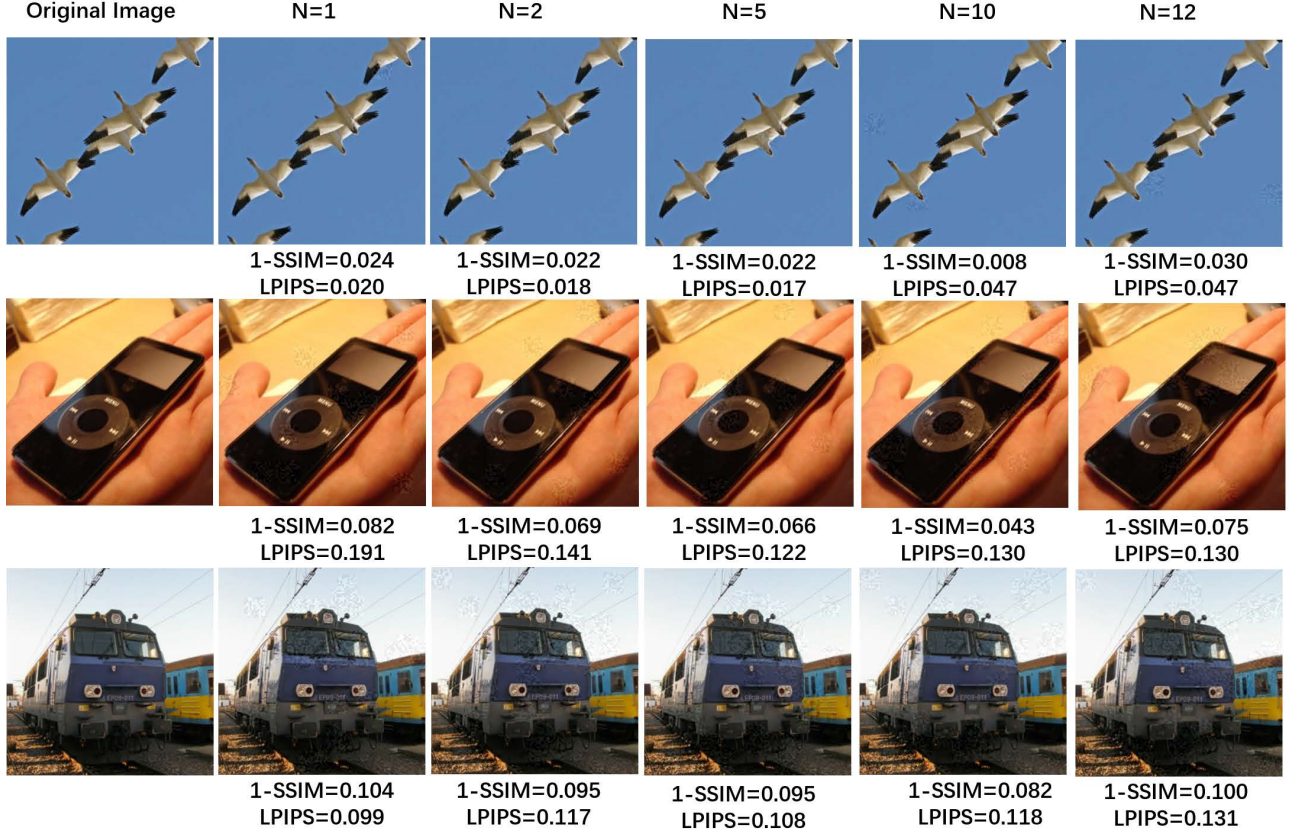


Figure 4: Adversarial examples under different sampling frequency. From left to right is the original image, the adversarial examples from $N = 1, 2, 5, 10, 12$, respectively.

Table 2: Results of the out-of-object attack on ImageNet when $\lambda = 10, N = 1$ and the perceptual distance metric being $1 - \text{SSIM}$. I, R and V represent InceptionV3, ResNet50 and VGG16bn, respectively.

Attacked Range	Success Rate			1 - SSIM			LPIPS			Avg. Queries		
	I	R	V	I	R	V	I	R	V	I	R	V
Image	100%	100%	100%	0.078	0.076	0.072	0.096	0.081	0.079	845	401	251
Out-of-object	90.1%	93.8%	94.7%	0.071	0.069	0.074	0.081	0.065	0.070	4275	3775	3104

Table 3: Comparison of the undefended (v3) and defended ($v3_{\text{adv-ens4}}$) InceptionV3. The defended InceptionV3 adopts ensemble adversarial training.

Network	Clean Accuracy	After Attack	1 - SSIM	LPIPS	Avg. Queries
v3	75.8%	0.8%	0.096	0.149	531
$v3_{\text{adv-ens4}}$	73.4%	1.8%	0.103	0.154	777

ensemble adversarial training (*i.e.*, $v3_{\text{adv-ens4}}$). Following [6], we set $\epsilon = 0.0625$ and randomly select 10,000 images from the ImageNet validation set for test. The maximum number of queries is 10,000. The performance of the attacked network is reported in Table 3, where clean accuracy is the classification accuracy before attack. Note that v3 is slightly different from InceptionV3 in Table 1 in that the pretrained model of v3 comes from Tensorflow, which is the same platform of the pretrained

model of $v3_{\text{adv-ens4}}$. Compared with undefended network, attacking defended one causes larger visual distortion. However, the proposed attack can still reduce the classification accuracy from 73.4% to 1.8%, which demonstrates its effectiveness under defend.

4.4 Comparison with Other Attacks

Different from previous work which focuses on query efficiency, our model addresses improving the visual similarity between the adversarial example and the original image. Therefore, the proposed method might cost more number of queries to construct a less distorted adversarial example. To show that such costs are affordable, we compare our attack to recently proposed query-efficient black-box attacks: SignHunter [8], NAttack [9], Bandits [5] and Square Attack [15]. Since these attacks do not consider visual distortion, for fair comparison, we add $1 - \text{SSIM}$

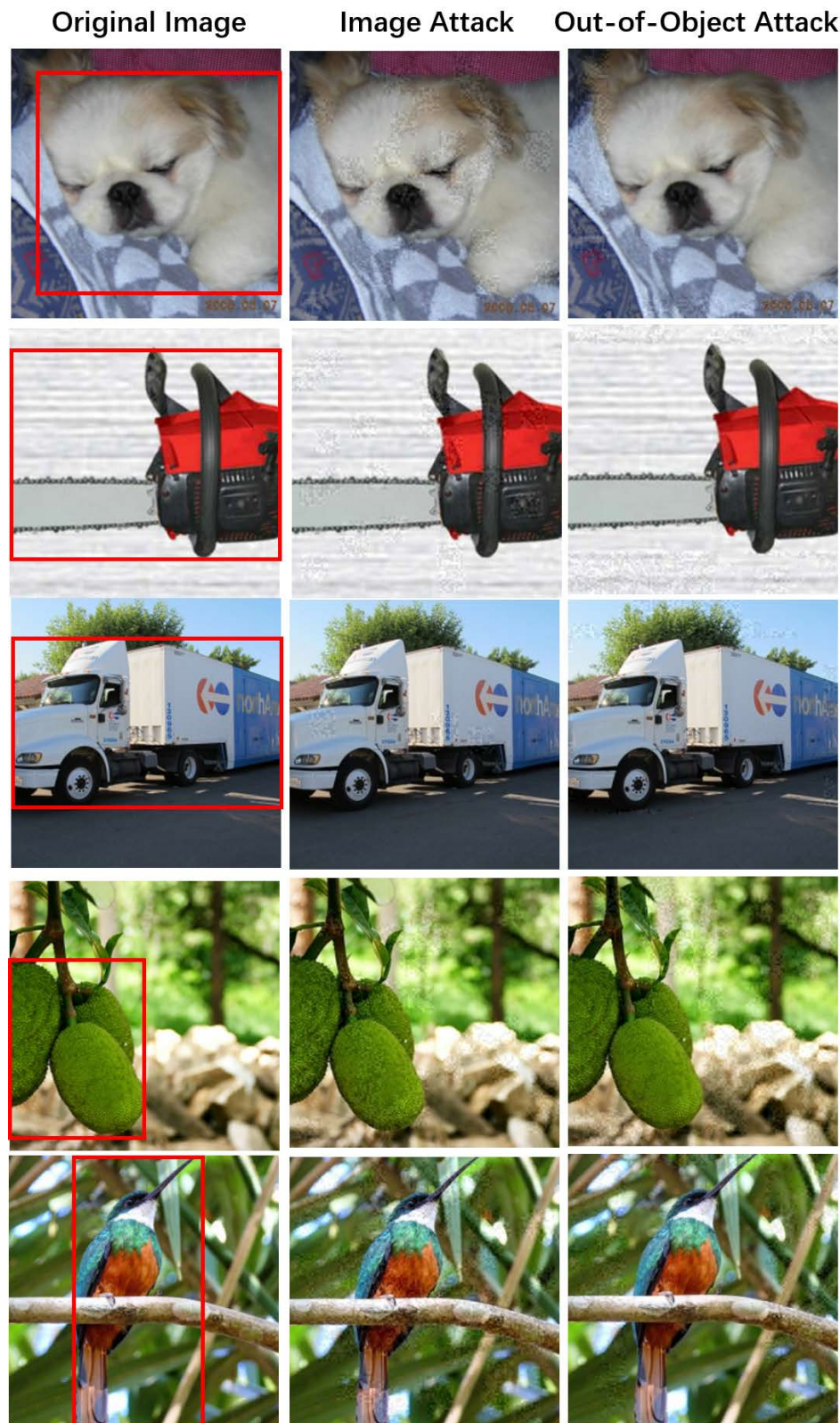


Figure 5: Visualized adversarial examples in out-of-object attack. The red bounding box locates the target object in the original image. In *out-of-object* attack, the adversary is only allowed to perturb pixels that are out of the object bounding box. In *image attack*, the adversary can perturb any pixel in the image.



Figure 6: Adversarial examples from different attacks with perceptual distance scores. From left to right is the original image, the adversarial examples from [5], [15], [8], [9] and our method, respectively.

Table 4: Results of different attacks on ImageNet. I, R and V represent InceptionV3, ResNet50 and VGG16bn, respectively.

Attack	Success Rate			1 – SSIM			LPIPS			Avg. Queries		
	I	R	V	I	R	V	I	R	V	I	R	V
SignHunter [8]	98.4%	-	-	0.157	-	-	0.117	-	-	450	-	-
NAttack [9]	99.5%	-	-	0.133	-	-	0.212	-	-	524	-	-
Bandits [5]	96.5%	98.8%	98.2%	0.343	0.307	0.282	0.201	0.157	0.140	935	705	388
Square Attack [15]	99.7%	100%	100%	0.280	0.279	0.299	0.265	0.243	0.247	237	62	30
SignHunter-SSIM	97.6%	-	-	0.220	-	-	0.157	-	-	642	-	-
NAttack-SSIM	97.3%	-	-	0.128	-	-	0.210	-	-	666	-	-
Bandits-SSIM	80.0%	89.3%	89.7%	0.333	0.303	0.275	0.200	0.163	0.135	1318	1020	793
Square Attack-SSIM	99.2%	100%	100%	0.260	0.268	0.292	0.256	0.238	0.245	278	65	30
Ours	98.7%	100%	100%	0.075	0.076	0.072	0.094	0.081	0.079	731	401	251

in their objective functions accordingly with $\lambda = 10$ as in our method, which are represented by -SSIM in Table 4. The results of the above methods are reproduced using the official codes provided by the authors. In NAttack, we set the sample size to be 10 since the original large sample size in the paper is computationally expensive. The maximum number of queries is 10,000 as in previous work. In our model, considering the trade-off between visual distortion and query efficiency, we set $\lambda = 10$, $N = 1$ and the perceptual distance metric to be 1 – SSIM. In Table 4, the proposed attack reduces 1 – SSIM and LPIPS approximately by half while remaining a high success rate (98.7%/100%/100%) within limited number of iterations. Except for Signhunter, introducing 1 – SSIM in the objective function helps reduce visual distortion in other attacks. However, our method still outperforms these attacks since the perceptual distance metric is *directly* minimized in our method. In addition, the number of queries of our attack is comparable to that of Bandits. Note that the success rates have a sharp decrease in Bandits-SSIM compared with Bandits. This is because Bandits attack uses estimated gradient of the black-box classifier as its prior, whereas simply adding 1 – SSIM in the loss causes inaccurate gradient. The visualized adversarial examples from different attacks are given in Fig. 6, which shows that our model produces less distorted adversarial examples. More examples can be found in Fig. 7.

We noticed that SignHunter produces adversarial examples with horizontal-stripped noise and Square Attack generates adversarial examples with vertical-stripped noise. Stripped noise is helpful in improving query efficiency since the classification network is quite sensitive to such noise [15]. However, from the perspective of visual distortion, such noise greatly degrades the image quality. The adversarial examples of Bandits are relatively

perceptible-friendly, but the perturbation affects most pixels in the image, which causes visually “noisy” effects, especially in a monochrome background. The noise produced by Nattack appear to be regular color patches all over the image due to its large tiling size in the method.

4.5 Other l_p Attacks

Although our method in this paper is based on l_∞ attack, other l_p ($p = 0, 1, 2$) distance can be regarded as the perceptual distance metric d in the loss function, which is minimized with a trade-off parameter λ . We did not discuss it in the experiments because these l_p distance metrics are less accurate in measuring the *perceptual* distance between images compared to the specifically designed metrics, such as well-established 1 – SSIM and LPIPS. In Table 5, the results of other l_p ($p = 0, 1, 2$) attacks are shown, where the l_p distance is normalized to $[0, 1]$ as the perceptual distance metric d in the loss function. Specifically, $d(x, x + \delta) = \frac{l_p(x, x + \delta)}{\max_\delta(l_p(x, x + \delta))}$, where $l_p(x, x + \delta)$ is the l_p distance between the original image x and the perturbed image $x + \delta$. As in the paper, we set $\lambda = 10$, $\epsilon = 0.05$ and the maximum number of queries being 10,000. We find that the raw l_0 and l_1 scores have much higher order of magnitude compared with other metrics, and thus the normalized scores of l_0 and l_1 distances are reported in Table 5. Note that when the sampling frequency $N = 1$, l_0 distance is equivalent to l_1 distance in that

$$\begin{aligned}
\frac{l_1(x, x + \delta)}{\max_\delta(l_1(x, x + \delta))} &= \frac{mc \cdot \epsilon}{whc \cdot \epsilon} \\
&= \frac{m}{wh} \\
&= \frac{l_0(x, x + \delta)}{\max_\delta(l_0(x, x + \delta))}
\end{aligned} \tag{22}$$

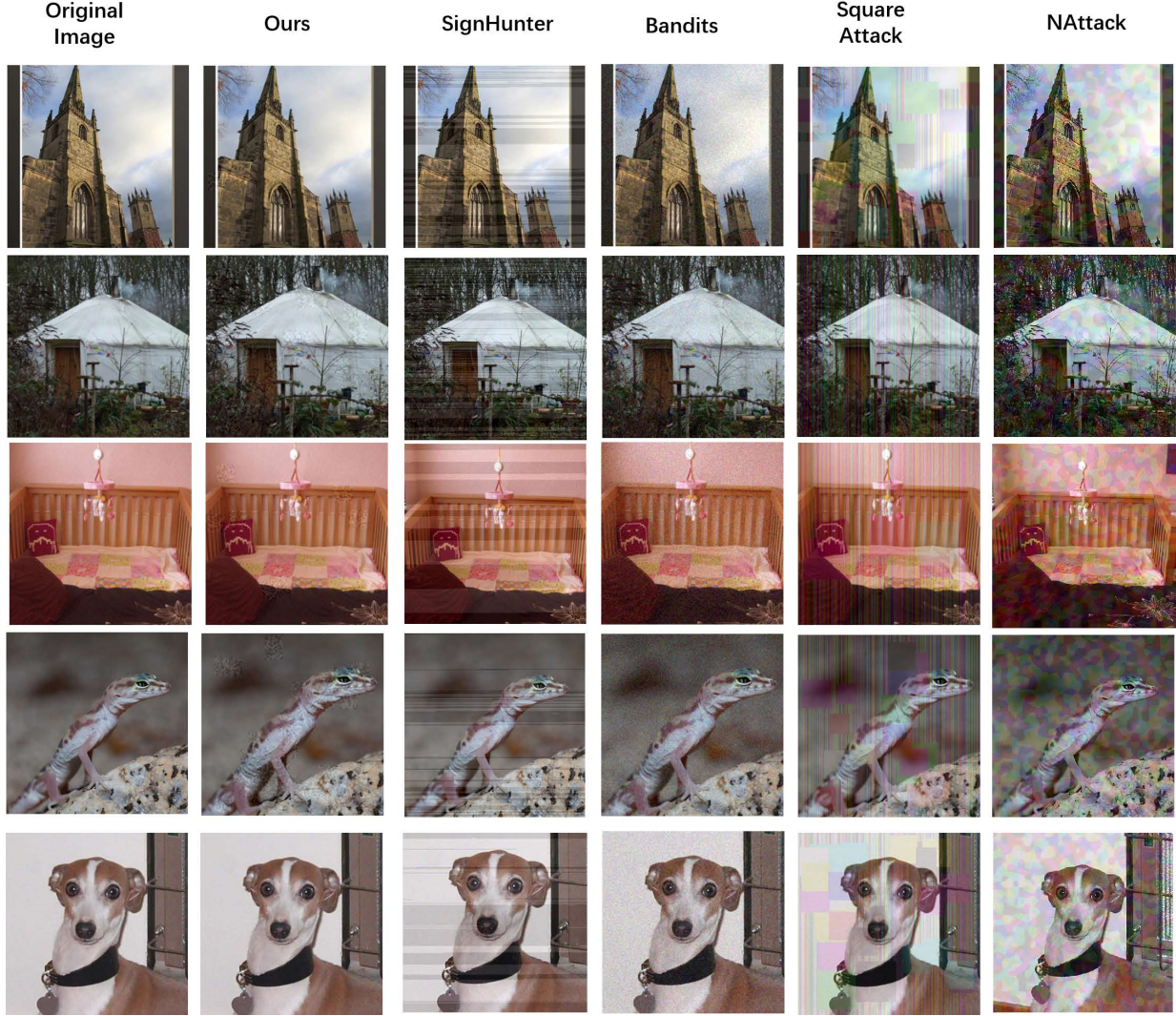


Figure 7: More visualized adversarial examples from different attacks.

Table 5: Results of other l_p attacks on ResNet50 when $\lambda = 10$. The raw l_0 and l_1 scores have much higher order of magnitude compared with other metrics, and thus the normalized scores of l_0 and l_1 distances are reported.

Distance Metric	Sampling Frequency	Success Rate	1 - SSIM	LPIPS	l_0	l_1	l_2	Avg. Queries
l_0	1	99.5%	0.077	0.083	0.133	0.130	6.75	536
	2	99.2%	0.065	0.069	0.159	0.118	5.88	679
	5	97.9%	0.058	0.065	0.177	0.118	5.19	960
l_1	1	99.5%	0.077	0.083	0.133	0.130	6.75	536
	2	99.5%	0.070	0.076	0.176	0.130	6.14	658
	5	99.2%	0.066	0.070	0.218	0.129	5.74	800
l_2	1	99.5%	0.110	0.112	0.215	0.211	8.21	392
	2	99.5%	0.092	0.100	0.259	0.191	7.44	431
	5	99.5%	0.087	0.094	0.312	0.185	6.89	579

where m is the number of perturbed pixels. w, h and c are the width, height and number of channels of a given image, respectively. Table 5 shows that optimizing l_0 distance gives better performance on both the perceptual distance metrics and the l_p distance metrics.

4.6 Conclusion

We introduce a novel black-box attack based on the induced visual distortion in the adversarial example. The quantified visual distortion, which measures the perceptual distance between the

adversarial example and the original image, is introduced in our loss where the gradient of the corresponding non-differentiable loss function is approximated by sampling from a learned noise distribution. The proposed attack can achieve a trade-off between visual distortion and query efficiency by introducing the weighted perceptual distance metric in addition to the original loss. The experiments demonstrate the effectiveness of our attack on ImageNet as our model achieves much lower distortion when compared to existing attacks. In addition, it is shown that our attack is valid even when it's only allowed to perturb pixels that are out of the target object in a given image.

REFERENCES

- [1] Nicholas Carlini and David A. Wagner. Towards evaluating the robustness of neural networks. In *IEEE Symposium on Security and Privacy*, 2017.
- [2] Alexey Kurakin, Ian J. Goodfellow, and Samy Bengio. Adversarial machine learning at scale. In *Proc. International Conference on Learning Representations*, 2017.
- [3] Nicolas Papernot, Patrick D. McDaniel, Ian J. Goodfellow, Somesh Jha, Z. Berkay Celik, and Ananthram Swami. Practical black-box attacks against machine learning. In *Proc. ACM on Asia Conference on Computer and Communications Security*, 2017.
- [4] Matt Jordan, Naren Manoj, Surbhi Goel, and Alexandros G. Dimakis. Quantifying perceptual distortion of adversarial examples. *arXiv preprint arXiv:1902.08265*, 2019.
- [5] Andrew Ilyas, Logan Engstrom, and Aleksander Madry. Prior convictions: Black-box adversarial attacks with bandits and priors. In *Proc. International Conference on Learning Representations*, 2019.
- [6] Florian Tramèr, Alexey Kurakin, Nicolas Papernot, Ian J. Goodfellow, Dan Boneh, and Patrick D. McDaniel. Ensemble adversarial training: Attacks and defenses. In *Proc. International Conference on Learning Representations*, 2018.
- [7] Chun-Chen Tu, Pai-Shun Ting, Pin-Yu Chen, Sijia Liu, Huan Zhang, Jinfeng Yi, Cho-Jui Hsieh, and Shin-Ming Cheng. AutoZOOM: Autoencoder-based zeroth order optimization method for attacking black-box neural networks. In *Proc. AAAI Conference on Artificial Intelligence*, 2019.
- [8] Abdullah Al-Dujaili and Una-May O'Reilly. Sign bits are all you need for black-box attacks. In *Proc. International Conference on Learning Representations*, 2020.
- [9] Yandong Li, Lijun Li, Liqiang Wang, Tong Zhang, and Boqing Gong. NATTACK: learning the distributions of adversarial examples for an improved black-box attack on deep neural networks. In *Proc. International Conference on Machine Learning*, 2019.
- [10] Shuyu Cheng, Yinpeng Dong, Tianyu Pang, Hang Su, and Jun Zhu. Improving black-box adversarial attacks with a transfer-based prior. In *Proc. International Conference on Neural Information Processing Systems*, 2019.
- [11] Nicolas Papernot, Patrick McDaniel, and Ian Goodfellow. Transferability in machine learning: from phenomena to black-box attacks using adversarial samples. *arXiv preprint arXiv:1605.07277*, 2016.
- [12] Ian J. Goodfellow, Jonathon Shlens, and Christian Szegedy. Explaining and harnessing adversarial examples. In *Proc. International Conference on Learning Representations*, 2015.
- [13] Seungyong Moon, Gaon An, and Hyun Oh Song. Parsimonious black-box adversarial attacks via efficient combinatorial optimization. In *Proc. International Conference on Machine Learning*, 2019.
- [14] Laurent Meunier, Jamal Atif, and Olivier Teytaud. Yet another but more efficient black-box adversarial attack: tiling and evolution strategies. *arXiv preprint arXiv:1910.02244*, 2019.
- [15] Maksym Andriushchenko, Francesco Croce, Nicolas Flammarion, and Matthias Hein. Square attack: a query-efficient black-box adversarial attack via random search. *arXiv preprint arXiv:1912.00049*, 2019.
- [16] Christian Szegedy, Wojciech Zaremba, Ilya Sutskever, Joan Bruna, Dumitru Erhan, Ian J. Goodfellow, and Rob Fergus. Intriguing properties of neural networks. In *Proc. International Conference on Learning Representations*, 2014.
- [17] Zhou Wang, A. C. Bovik, H. R. Sheikh, and E. P. Simoncelli. Image quality assessment: from error visibility to structural similarity. *IEEE Transactions on Image Processing*, 13(4):600–612, 2004.
- [18] Richard Zhang, Phillip Isola, Alexei A. Efros, Eli Shechtman, and Oliver Wang. The unreasonable effectiveness of deep features as a perceptual metric. In *Proc. IEEE Conference on Computer Vision and Pattern Recognition*, 2018.
- [19] Richard S Sutton and Andrew G Barto. *Reinforcement learning: An introduction*. MIT press Cambridge, 1998.
- [20] Wenjie Ruan, Xiaowei Huang, and Marta Kwiatkowska. Reachability analysis of deep neural networks with provable guarantees. In *Proc. International Joint Conference on Artificial Intelligence*, 2018.
- [21] Bolin Gao and Laca Pavel. On the properties of the softmax function with application in game theory and reinforcement learning. *arXiv preprint arXiv:1704.00805*, 2017.
- [22] Ryan Tibshirani. Gradient descent: Convergence analysis, 2013. <https://www.stat.cmu.edu/~ryantibs/convexopt-F13/scribes/lec6.pdf>.
- [23] Olga Russakovsky, Jia Deng, Hao Su, Jonathan Krause, Sanjeev Satheesh, Sean Ma, Zhiheng Huang, Andrej Karpathy, Aditya Khosla, Michael Bernstein, Alexander C. Berg, and Li Fei-Fei. ImageNet Large Scale Visual Recognition Challenge. *International Journal of Computer Vision*, 115(3):211–252, 2015.
- [24] Christian Szegedy, Vincent Vanhoucke, Sergey Ioffe, Jonathon Shlens, and Zbigniew Wojna. Rethinking the inception architecture for computer vision. In *Proc. IEEE Conference on Computer Vision and Pattern Recognition*, 2016.
- [25] Kaiming He, Xiangyu Zhang, Shaoqing Ren, and Jian Sun. Deep residual learning for image recognition. In

Proc. IEEE Conference on Computer Vision and Pattern Recognition, 2016.

- [26] Karen Simonyan and Andrew Zisserman. Very deep convolutional networks for large-scale image recognition. In *Proc. International Conference on Learning Representations*, 2015.
- [27] Jie Hu, Li Shen, and Gang Sun. Squeeze-and-excitation networks. In *Proc. IEEE Conference on Computer Vision and Pattern Recognition*, 2018.